

# On the choice of training data for machine learning of geostrophic mesoscale turbulence

F. E. Yan<sup>1</sup>, J. Mak<sup>1,2</sup>, Y. Wang<sup>1,2</sup>

<sup>1</sup>Department of Ocean Science, Hong Kong University of Science and Technology

<sup>2</sup>Center for Ocean Research in Hong Kong and Macau, Hong Kong University of Science and Technology

## Key Points:

- Investigate dependence of convolution neural network's on choice of training data for geostrophic turbulence
- Eddy force function used as a way to filter out dynamically inert eddy fluxes
- Models trained on filtered eddy fluxes at least as accurate but more robust than models trained on the divergence of eddy fluxes

arXiv:2307.00734v1 [physics.ao-ph] 3 Jul 2023

---

Corresponding author: Fei Er Yan, [feyan@connect.ust.hk](mailto:feyan@connect.ust.hk)

Corresponding author: Julian Mak, [julian.c.l.mak@gmail.com](mailto:julian.c.l.mak@gmail.com)

**Abstract**

‘Data’ plays a central role in data-driven methods, but is not often the subject of focus in investigations of machine learning algorithms as applied to Earth System Modeling related problems. Here we consider the case of eddy-mean interaction in rotating stratified turbulence in the presence of lateral boundaries, a problem of relevance to ocean modeling, where the eddy fluxes contain dynamically inert rotational components that are expected to contaminate the learning process. An often utilized choice in the literature is to learn from the divergence of the eddy fluxes. Here we provide theoretical arguments and numerical evidence that learning from the eddy fluxes with the rotational component appropriately filtered out results in models with comparable or better skill, but substantially improved robustness. If we simply want a data-driven model to have predictive skill then the choice of data choice and/or quality may not be critical, but we argue it is highly desirable and perhaps even necessary if we want to leverage data-driven methods to aid in discovering unknown or hidden physical processes within the data itself.

**Plain Language Summary**

Data-drive methods and machine learning are increasingly being utilized in various problems relating to Earth System Modeling. While there are many works focusing on the machine learning algorithms or the problems themselves, there has been relative few investigations into the impact of data choice or quality, given the central role the data plays. We consider here the impact of data choice for a particular problem of eddy-mean interaction of relevance to ocean modeling, and provide theoretical arguments and numerical evidence to suggest that one choice (informed by our theoretical understanding of the underlying problem) is preferable over a more standard choice utilized in the literature. While the choice of data choice and/or quality may not be critical if we simply want a data-driven model to ‘work’, we argue it is highly desirable (possibly even a necessity) if we want to go beyond having models that just ‘work’, such as leveraging data-driven methods to help us in discovering unknown or hidden physical processes within the data itself.

**1 Introduction**

Data-driven methods and machine learning algorithms are increasingly being utilized in problems relating to Earth system and/or climate modeling, and there is no doubt such methods have a strong potential in greatly enhancing model skill and/or reducing computation cost in various numerical models. Some examples of usage includes dynamical processes in the atmosphere (e.g., Brenowitz & Bretherton, 2019; Yuval & O’Gorman, 2020; Mooers et al., 2021; Connolly et al., 2023; Sun et al., 2023), climate modeling (e.g., Besombes et al., 2021; Sonnewald & Lguensat, 2021), see ice prediction (e.g., Bolibar et al., 2020; Andersson et al., 2021), identification problems in oceanography (e.g., Jones et al., 2019; Thomas et al., 2021; Sonnewald et al., 2019, 2023), and our primary focus here, on ocean mesoscale turbulence (e.g., Bolton & Zanna, 2019; Zanna & Bolton, 2021; Guillaumin & Zanna, 2021). We refer the reader to the works of Reichstein et al. (2019), Irrgang et al. (2021), Sonnewald et al. (2021) and Camps-Valls et al. (2023) for a more comprehensive review.

One criticism of some data-driven methods and machine learning algorithms is the ‘black-box’ nature of the resulting models. In general, for a problem with input  $x$  and output  $y$ , a focus of data-driven methods is to find some mapping  $f$  such that  $f(x) = y$ , where  $f$  could be deterministic or probabilistic depending on the algorithm used to obtain  $f$ . The lack of interpretability for  $f$  in certain instances brings into question several important issues with the use of data-driven methods. The first is robustness and applicability in different regimes: are the models doing the right things for the ‘right’

reasons (or at least not the ‘wrong’ ones)? If for the ‘wrong’ reasons, then it is perfectly plausible that trained up models can behave erratically when taken outside the trained regimes and, given the nonlinear and convoluted nature of the model itself, generate subtly wrong results that might be close to impossible to check. The second relates to further utilities of the methods themselves: is it possible to use such methods to aid process discovery from the data itself? A lack of interpretability would suggest a negative answer to that question. With that in mind, there has been an increasing focus on physically constrained and/or interpretable/explainable models (e.g., Zhang & Lin, 2018; Brenowitz et al., 2020; Zanna & Bolton, 2021; Beucler et al., 2021; Kashinath et al., 2021; Sonnewald & Lguensat, 2021; Yuval et al., 2021; Barnes et al., 2022; Clare et al., 2022; Lopez-Gomez et al., 2022; Guan et al., 2023). While the tools and algorithms do exist, this is a fundamentally harder problem, since the training step ultimately becomes one of a constrained optimization problem.

While the algorithms and nature of the resulting model  $f$  (e.g. linear vs. nonlinear, generative vs. discriminative, model complexity) are important details, at the very base level we are really dealing with the problem of *data regression*. We would thus expect *data choice* and/or *data quality* to critically affect the training, the performance or the useful information that could be extracted/encoded by the model, but are issues that have not received much investigation. If we simply want a model that ‘works’ in the sense of producing a ‘skilled’ prediction in whatever metric we think is relevant, then the issue of data quality and/or content may not be critical, since we are simply looking for some optimal fit. If on the other hand we are interested in the harder problem of optimal fit with constraints, such as having a model that works for the ‘right’ reasons (e.g. satisfying physical conservation laws), or using data-driven methods for process discovery (e.g. telling us about the underlying physics of a problem), then one might imagine the choice and quality of data exposed to the model should be important. Furthermore, certain data may be more accessible for the machine learning algorithms to extract/predict features from (e.g. smoothness and/or spatio-temporal scale of data), which has practical consequences for the optimization procedure at the model training and prediction step.

To demonstrate that not all choices of data are equal, we consider in this work the problem of eddy-mean interaction in rotating stratified turbulence in the presence of boundaries, a setting that is particularly relevant to ocean modeling and parameterization of geostrophic mesoscale eddies. The problem relates to the presence of rotational fluxes (e.g. J. C. Marshall & Shutts, 1981; Fox-Kemper et al., 2003; Maddison et al., 2015), and we provide some theoretical arguments and evidence on why learning from the *eddy force function*, which is one method to deal with the presence of dynamically inert rotational fluxes, might be preferable to learning from the divergence of the eddy fluxes. We will largely leverage the experimental procedure of Bolton and Zanna (2019), albeit with important differences to be detailed. While the present investigation is largely empirical and relies on input of external knowledge that is somewhat specific to the present problem, the present work serves to open a discussion into data choice and/or quality, as well as probing the available information content in data in the general case, possibly in a more systematic and objective fashion than one performed here.

The technical problem statement relating to rotational fluxes and its plausible impact on data quality for data-driven methods are outlined in §2. In §3 we outline our experimental procedure, numerical model used and data-driven method. §4 summarizes the impact of data choice on the skill of the trained models. §5 considers the issue of model robustness via investigating the models’ skill and their sensitivity to noise in the training data. We close in §6 and provide outlooks, focusing particularly on further experiments to probe the information content of data being for use in data-driven methods of relevance to the present eddy-mean interaction problem.

## 2 Rotational fluxes and the eddy force function

### 2.1 Formulation

For this particular work we consider turbulent motion under the influence of strong rotation and stratification. Specifically, we consider the Quasi-Geostrophic (QG) limit (e.g. Vallis, 2006), which is a widely-used and applicable limit for oceanic mesoscale dynamics where the motion is geostrophic at leading order. If we consider the standard Reynolds decomposition with

$$A = \overline{A} + A', \quad \overline{A + B} = \overline{A} + \overline{B}, \quad \overline{A'} = 0, \quad (1)$$

where the overbar denotes a mean (with the projection operator assumed to commute with all relevant derivatives), and a prime denotes a deviation from the mean, the mean QG Potential Vorticity (PV) equation takes the form

$$\frac{\partial \overline{q}}{\partial t} + \nabla \cdot (\overline{\mathbf{u}q}) = -\nabla \cdot \overline{\mathbf{u}'q'} + \overline{Q}. \quad (2)$$

Here,  $t$  denotes the time,  $\nabla$  denotes the horizontal gradient operator, so that the PV  $q$  is defined as

$$q = \nabla^2 \psi + \beta y + \frac{\partial}{\partial z} \frac{f_0}{N_0^2} \frac{\partial b}{\partial z}, \quad (3)$$

where  $\psi$  is the streamfunction,  $f = f_0 + \beta y$  is the Coriolis frequency (background value and leading order meridional variation),  $N_0$  is the (static) buoyancy frequency related to the imposed background stratification,  $b = f_0 \partial \psi / \partial z$  is the buoyancy,  $\mathbf{u} = \nabla^\perp \psi = (-\partial \psi / \partial y, \partial \psi / \partial x)$  is the non-divergent geostrophic velocity, and  $Q$  represents all forcing and dissipation.

An aim in studies of eddy-mean interaction is to understand the inter-dependence of the nonlinear eddy flux terms on the right hand side of Eq. (2) and the mean state. A particular goal with eddy parameterization is to relate the eddy flux term  $\overline{\mathbf{u}'q'}$  with some large-scale mean state, normally as

$$\overline{\mathbf{u}'q'} \sim f(\overline{q}, \dots; \kappa, \dots), \quad (4)$$

where  $f$  is some mapping between mean states (such as  $\overline{q}$ ) and associated parameters (such as  $\kappa$ ) to the eddy fluxes. Once such a relation exists, we take a divergence, from which we obtain the eddy forcing on the mean. A notable example would be PV diffusion (e.g., Green, 1970; J. C. Marshall, 1981; Rhines & Young, 1982), where we directly postulate for the form of  $F$  as

$$\overline{\mathbf{u}'q'} = -\kappa \nabla \overline{q} \quad \Rightarrow \quad -\nabla \cdot \overline{\mathbf{u}'q'} = \nabla \cdot (\kappa \nabla \overline{q}). \quad (5)$$

We emphasize the ordering of the operations here: we obtain a functional relation between the mean and eddy fluxes first, then we take a divergence to obtain the eddy forcing (cf. Fickian diffusion closures).

### 2.2 The issue of rotational fluxes

The form as given in Eq. (4) is suggestive that data-driven approaches would be useful by either directly regressing/learning for the mapping  $f$ , or when a mapping (cf. parameterization) such as Eq. (5) is given, to learn for the parameters such as  $\kappa$ . However, there is a subtlety involved here, arising from the fact that it is the divergence of the eddy fluxes that arises (and is generic beyond the QG system, where the eddy forcing arises from a divergence of the Eliassen–Palm flux tensor, with the eddy fluxes as the tensor components, e.g. Young, 2012; Maddison & Marshall, 2013). A two-dimensional vector field such as  $\overline{\mathbf{u}'q'}$  can, via a Helmholtz decomposition, be written as

$$\overline{\mathbf{u}'q'} = \nabla \tilde{\Psi} + \hat{\mathbf{e}}_z \times \nabla \tilde{\Phi} + \tilde{\mathbf{H}}, \quad (6)$$

where  $\hat{e}_z$  is the unit vector pointing in the vertical, and the terms are respectively a divergent (vanishing under a curl), rotational (vanishing under a divergence), and harmonic component (vanishing under both a curl and divergence). Since the eddy forcing on the mean appears as a divergence, the rotational (and harmonic) eddy fluxes are dynamically inert, and one might expect that the presence of such dynamically inert fluxes is going to be detrimental to the regression/learning by data-driven methods. Similar issues arise for example arise in a diagnostic problem for the PV diffusivity  $\kappa$ , where rotational fluxes are known to severely contaminate the calculation (e.g. Fig.1 Mak et al., 2016).

One way to get around this problem is to perform a Helmholtz decomposition as above and only perform learning/regression/diagnoses using only the divergent term  $\nabla\tilde{\Psi}$ . This approach is however complicated by the issue of gauge freedom in the presence of boundaries (e.g., Fox-Kemper et al., 2003; Maddison et al., 2015; Mak et al., 2016). The standard Helmholtz decomposition as commonly employed (e.g. in electromagnetism problems) is unique because we have periodic or rapidly decaying boundary conditions. The non-uniqueness of the Helmholtz decomposition in the presence of boundaries arises from the fact that there is generically no inherited natural boundary condition for arbitrary choices of vector fields (although there may be ones that are physically relevant depending on the problem), and that the divergent term  $\nabla\tilde{\Psi}$  is unique only up to an arbitrary rotational gauge.

One possibility might be to utilize the divergence of the eddy flux directly (e.g.  $\nabla\cdot\overline{\mathbf{u}'q'}$ ). This is somewhat the approach taken for example in the works of Bolton and Zanna (2019) and Zanna and Bolton (2021), who considers applying data-driven methods to learn about sub-grid momentum forcing in an ocean relevant model. While they report positive results from data-driven methods in their work, there are some points that are worth revisiting, particularly regarding learning from the divergence of the eddy flux. One issue is the spatial resolution of data itself: the eddy flux data itself is already small-scale, and now we want its divergence, which is an even finer scale quantity, so there could be sensitivity of the data to the numerical model resolution itself. Following on from this point is the issue of *robustness*. The learning problem here is trying to find a mapping between very small-scale data and large-scale data (e.g., divergence of eddy flux and say some function of the streamfunction), and questions arise whether this leads to sensitivity to the training data, or whether such a choice is unnecessarily taxing on the machine learning algorithms. A final point is more subtle and more speculative, to do with *commutativity*, i.e. ordering of operations. Eddy parameterizations are usually formulated as in Eq. (4): we learn a  $f(\dots) = \overline{\mathbf{u}'q'}$ , from which we take a divergence of the learned  $f$  to get the eddy forcing. If we are learning from  $\nabla\cdot\overline{\mathbf{u}'q'}$ , then the ordering is different, because we are really learning for some  $\nabla\cdot\overline{\mathbf{u}'q'} = \hat{f}(\dots)$ , where we would hope that  $\hat{f} = \nabla\cdot F$ . There is however no reason to expect such an equality in general, since the resulting mappings  $F$  or  $\hat{F}$  obtained from machine learning algorithms are nonlinear.

If we are simply interested in something that just ‘works’, then these aforementioned points may not actually matter. If, on the other hand, we are interested in learning about the underlying physics via data-driven methods, then it is not clear whether the aforementioned properties (or the lack thereof) become fundamental limitations in the applicability of the procedure.

### 2.3 The eddy force function

If we instead consider learning from data at the eddy flux level, then we probably want to filter out the rotational component in some way, ideally in a unique fashion. While the statement about the non-uniqueness of the Helmholtz decomposition holds for generic tracer fluxes in the presence of boundaries, it turns out, for the QG system and for the

eddy PV flux, there is in fact a natural boundary condition that is inherited from the no-normal flow condition (Maddison et al., 2015). The decomposition

$$\overline{\mathbf{u}'q'} = -\nabla\Psi_{\text{eff}}^q + \hat{\mathbf{e}}_z \times \nabla\Phi_{\text{eff}}^q + \mathbf{H}^q, \quad (7)$$

where  $\Psi_{\text{eff}}^q$  denotes the eddy force function (note the extra minus sign on the gradient term compared to Eq. 6), and may be obtained from solving the Poisson equation

$$\nabla \cdot \overline{\mathbf{u}'q'} = -\nabla^2\Psi_{\text{eff}}^q \quad (8)$$

subject to homogeneous Dirichlet boundary conditions  $\Psi_{\text{eff}}^q = 0$ . Such an object is uniquely defined (from fixing the gauge freedom via the naturally inherited boundary condition), and  $\Psi_{\text{eff}}^q$  can be proved to be optimal in the  $H_0^1$  sense, i.e.  $-\nabla\Psi_{\text{eff}}^q$  is a minimizer in  $L^2$ , or that the dynamically active part of the eddy flux encoded by divergent part is as ‘uncontaminated’ as possible, at least in a simply connected domain (see Appendix A of Maddison et al., 2015). Furthermore, via the linearity assumption of the eddy force function and boundary condition inheritance (Maddison et al., 2015), we can define an eddy force function for the components that contribute towards the definition of eddy PV flux: for example, from the definition of PV given in Eq. (3), we can decompose

$$\overline{\mathbf{u}'\zeta'} = -\nabla\Psi_{\text{eff}}^\zeta + \hat{\mathbf{e}}_z \times \nabla\Phi_{\text{eff}}^\zeta + \mathbf{H}^\zeta, \quad (9)$$

where  $\zeta = \nabla^2\psi$  is the relative vorticity, giving rise to a relative vorticity or momentum eddy force function  $\Psi_{\text{eff}}^\zeta$  (related to the Reynolds stress via the Taylor identity, e.g. Maddison & Marshall, 2013), computed via an analogous Poisson equation to Eq. (8) also with homogeneous Dirichlet boundary conditions, and similarly for a buoyancy eddy force function  $\Psi_{\text{eff}}^b$ . For concreteness, the discussion will focus on the PV eddy force function  $\Psi_{\text{eff}}^q$ , but we document results from all three contributions in the later sections.

The eddy force functions have been previously demonstrated to be a useful quantity for diagnoses problems (e.g., Mak et al., 2016, in diagnosing eddy diffusivities via inverse approaches), and we might expect that it would be a useful quantity for data-driven methods applied to eddy parameterization of rotating stratified turbulence. To compare with the discussion above, the eddy force function is a larger-scale object, which might lead to weaker sensitivity during the training phase compared to training on  $\nabla \cdot \overline{\mathbf{u}'q'}$ . The gradient of the eddy force function  $-\nabla\Psi_{\text{eff}}^q$  uniquely defines the dynamically relevant eddy flux, suggesting that  $-\nabla\Psi_{\text{eff}}^q$  would serve as a better choice of data compared to training on  $\overline{\mathbf{u}'q'}$ , since the latter contains dynamically irrelevant data. Additionally, given parameterizations are more naturally formulated as a relation between the eddy fluxes and the mean state (cf. Eq. 4),  $-\nabla\Psi_{\text{eff}}^q$  avoids the possible issue with commutativity mentioned above.

### 3 Model details

Taking into account the above discussion, we explore here whether the eddy force function serves as a potentially useful object for machine learning of ocean mesoscale turbulence. For a problem  $y = f(x)$ , the focus here is principally on the skill of the models  $f$ , trained on various output data  $y$  for the same inputs  $x$ , where skill is to be measured by various mismatches between  $y_{\text{data}}$  and  $y_{\text{predict}} = f(x_{\text{data}})$ . We detail here a set of experiments to test and explore the following hypotheses:

1. models trained upon the filtered eddy flux  $-\nabla\Psi_{\text{eff}}^q$  would be more skillful than ones trained upon the full eddy flux  $\overline{\mathbf{u}'q'}$ ,
2. models trained upon the filtered eddy flux  $-\nabla\Psi_{\text{eff}}^q$  would possibly be comparable in skill to ones trained upon the divergence of the eddy flux  $\nabla \cdot \overline{\mathbf{u}'q'}$ , but the latter models might be more sensitive to data quality.

The experimental approach will largely mirror that of Bolton and Zanna (2019). However, one important fundamental difference of our work is the choice of average, which impacts the definition of eddies from Eq. (1). Where Bolton and Zanna (2019) take a low-pass spatial filter as the projection operator, here we employ a time-average and has the property that  $\overline{A'} = 0$  in line with properties of a Reynolds operator. Our eddy forcing then is in the more familiar form of a nonlinear eddy flux (e.g.  $\nabla \cdot \overline{\mathbf{u}'q'}$ ), rather than as a difference between the spatially averaged quantities (e.g.,  $\mathbf{S} = \nabla \cdot (\overline{\mathbf{u}q}) - \nabla \cdot (\overline{\mathbf{u}}\overline{q})$ , Eq. 7 of Bolton & Zanna, 2019). The current definition of the eddy force function  $\Psi_{\text{eff}}^q$  assumes a Reynolds average (Maddison et al., 2015), and while there are likely extensions and relaxation of assumptions possible, for simplicity we do not pursue this avenue and utilize time-averaging.

### 3.1 Numerical ocean model setup

The physical setup we consider is essentially the same three-layer QG square double gyre configuration as Bolton and Zanna (2019) (cf. Berloff, 2005; Karabasov et al., 2009; D. P. Marshall et al., 2012; Mak et al., 2016), but solved with a pseudo-spectral method instead of using the finite difference CABARET scheme of Karabasov et al. (2009). The numerical model (`qgm2`) generating the data presented in this work utilizes the parameters detailed in Mak et al. (2016), with the stratification parameters chosen such that the first and second Rossby deformation radii are 32.2 and 18.9 km, with a horizontal grid spacing of  $\Delta x = \Delta y = 7.5$  km (which is 512 by 512 in horizontal grid points), a horizontal viscosity value of  $\nu = 50 \text{ m}^2 \text{ s}^{-1}$ , and a time-step of  $\Delta t = 30$  mins. A wind forcing with peak wind stress of  $\tau_0 = 0.8 \text{ N m}^{-2}$  is used (correcting a typo in Table 1 of Mak et al., 2016). The model is spun up from rest for 20,000 days, and a further integration period of 5,000 days after this spin up is performed for computing time-averages.

The accumulated time-averages of the eddy fluxes are used to compute the eddy force function  $\Psi_{\text{eff}}$  via solving the Poisson equation in Eq. (8) with homogeneous Dirichlet boundary conditions, performed per layer. For this procedure, we leverage the FEniCS software (Logg & Wells, 2010; Logg et al., 2012; Alnæs et al., 2014) following the previous works of Maddison et al. (2015) and Mak et al. (2016), making use of the high level abstraction, automatic code generation capabilities and the numerous inbuilt solvers that are particularly suited to elliptic equations we have here. The data from each grid point of the numerical model are the nodal values on a regular structured triangular mesh, with a projection onto a piecewise linear basis (CG1). All derivative operations are performed on the finite element mesh, and the nodal values of the relevant fields are restructured into arrays for feeding into the machine learning algorithms.

Fig. 1 shows some sample output data in the surface layer. The two horizontal components of the time-averaged eddy PV fluxes in panels (b, c) are the datasets returned by the numerical model, which is sampled onto a finite element mesh as a vector object. The resulting object's divergence can then be computed, and the result is given in panel (a). As expected, the divergence of the eddy PV flux has more smaller-scale fluctuations and is less smooth than the eddy PV fluxes. Solving the relevant Poisson equation in FEniCS, the PV eddy force function  $\Psi_{\text{eff}}^q$  is shown in panel (d). From Maddison et al. (2015), the gradient of the eddy force function  $\nabla \Psi_{\text{eff}}^q$  has a physical interpretation when considered together with the time-mean streamfunction  $\overline{\psi}$  (not shown, but see Maddison et al., 2015), interpreted as whether eddies are accelerating the mean-flow (if  $\nabla \Psi_{\text{eff}}^q \cdot \nabla \overline{\psi} > 0$ , interpreted as an input of energy into the mean by eddies) or decelerating the mean flow (if  $\nabla \Psi_{\text{eff}}^q \cdot \nabla \overline{\psi} < 0$ , interpreted as an extraction of energy from the mean by eddies). Here, the eddy force function can be shown to correspond to the regimes where the eddies are slowing down the mean-flow via baroclinic instability when the Western Boundary Current first separates (the first positive-negative pattern emanating from the western boundary, which is anti-correlated with  $\nabla \overline{\psi}$ ), while the next dipole pattern (the first negative-positive patterns, which is correlated with  $\nabla \overline{\psi}$ ) is an eddy forcing of the

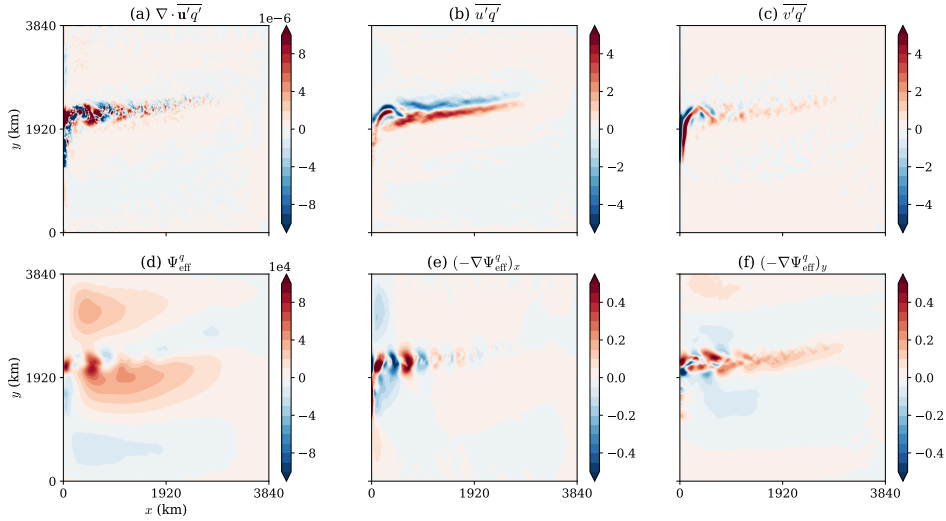


**Figure 1.** (a) The divergence of the eddy PV flux (units of  $\text{s}^{-2}$ ), calculated from the diagnosed time-averaged (b) zonal and (c) meridional component of the PV fluxes (units of  $\text{m s}^{-2}$ ). (d) The associated eddy force function  $\Psi_{\text{eff}}^q$  (units of  $\text{m}^2 \text{s}^{-2}$ ) calculated from the data shown in panel a, and the (e) zonal and (f) meridional component of  $-\nabla\Psi_{\text{eff}}^q$ , the associated eddy PV fluxes with the dynamically inert rotational component removed (units of  $\text{m s}^{-2}$ ). Note the different choices of colorbar limits between the data range in panels (b, c) and (e, f).

mean-flow corresponding to an eddy driven regime (cf. Waterman & Jayne, 2011; Waterman & Hoskins, 2013).

From this  $\Psi_{\text{eff}}^q$ , the horizontal components of the gradient leads to the eddy PV fluxes with the rotational component removed, and are shown in panels (e, f). While not obvious at first sight, the divergence of the full eddy PV flux (panels b, c) and the divergence of the filtered eddy PV flux (panels e, f) are both equal to  $\nabla\cdot\overline{\mathbf{u}'q'}$  (panel a) up to numerical solver errors (here at least four orders of magnitude smaller than the data). In this instance, note also that the filtered eddy flux has qualitatively different spatial patterns to the full eddy flux, and that the filtered eddy flux is around an order of magnitude smaller than the full eddy fluxes. The behavior is consistent with observations that the rotational eddy fluxes can be large (e.g. Griesel et al., 2009), and suggests we probably do want to filter the dynamically inert component out should we utilize eddy flux data to learn about geostrophic turbulence.

### 3.2 Model training procedure

Following Bolton and Zanna (2019) we employ Convolutional Neural Networks (CNNs; e.g., §9, Goodfellow et al., 2016) to map between the specified inputs and targets. In line with the intended investigation, the choice of parameters for training the CNNs are kept fixed and chosen as in Bolton and Zanna (2019), and the main quantity we vary is the choice of output data. The mappings that are returned as a CNN are denoted:

- $f_{\text{div}}^q(\dots)$ , with output data as the divergence of the eddy PV flux  $\nabla\cdot\overline{\mathbf{u}'q'}$ ,
- $f_{\text{full}}^q(\dots)$ , with output target data as the full eddy PV flux  $\overline{\mathbf{u}'q'}$ ,
- $f_{\text{eff}}^q(\dots)$ , with output data as the dynamically active eddy PV flux as defined through a gradient of the PV eddy force function (cf. Eq. 8)  $-\nabla\Psi_{\text{eff}}^q$ .

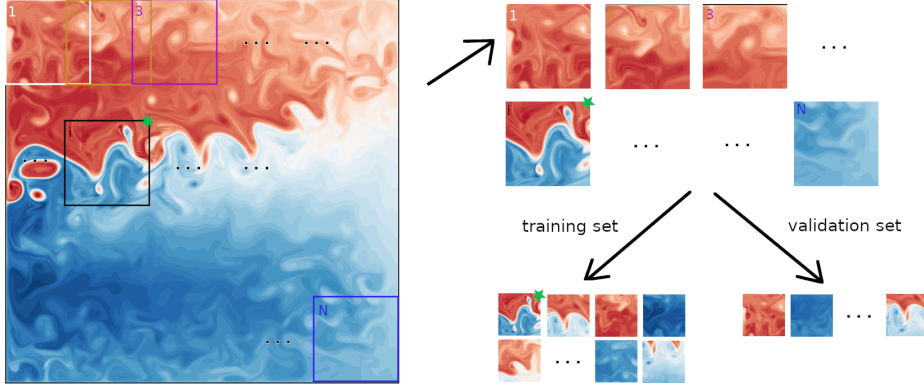


**Figure 2.** Model training strategy demonstrated here with a snapshot of the instantaneous PV from model output. The domain is partitioned into small square regions of size 40 by 40 pixels, overlapping in the  $x$  and  $y$  direction by 6 pixels, resulting in 6400 entries of input and output data. Each pair of input and output data is assigned with equal probability to be in the training set and validation set at the 80:20 ratio, from which a trained model results. An ensemble of models with 20 members is created, and are tested according to the procedure detailed in text.

Note that  $f_{\text{div}}^q(\dots)$  predicts a scalar field, while the  $f_{\text{full/eff}}^q(\dots)$  returns a vector field. A possible choice could be to train a model from the eddy force function, and from the trained model’s predicted eddy force function compute its Laplacian to obtain the divergence of the eddy flux. As mentioned above, this is an extremely difficult test for model skill since gradient operations amplify mismatches, and we comment on related results and observations are in the conclusions section.

To train up these mappings in the present time-averaged case, we follow the schematic given in Fig. 2, partially inspired by the approach of Bolton and Zanna (2019). The model domain is partitioned into small overlapping boxes. The input and output data associated with each of these boxes are paired up, and the pairs are each assigned a number and randomly shuffled (i.e. sampling from a uniform probability distribution function) depending on a choice of a random seed, and subsequently assigned to the training set (for training up the model) and validation (for tuning the hyperparameters in order to minimize a specified loss function) set with a 80:20 ratio. A model is trained up, and the skill of the model is its ability to be able to predict the global field. In the 512 by 512 pixel domain, we take the small boxes to be 40 by 40 pixels, with a stride of six, resulting in a collection of  $80^2 = 6400$  images of the domain. For statistical significance, an ensemble of 20 such models were trained up, each ensemble member only differing in the choice of the random seed, and the same sets of random seeds are used for the ensembles to be compared against. The CNNs are built using the PyTorch platform (Paszke et al., 2019), where the CNN architecture consists of three hidden convolutional layers with square kernels (of size 8, 4 and 4 respectively), with a two-dimension max pooling layer with square kernel of size 2, and a fully-connected linear activation layer as the output. The CNNs are trained with a batch size of 64, using the Adam optimizer (Kingma & Ba, 2015) with a mean squared error loss function. An early stopping criterion is used to monitor the loss function during the training to avoid over-fitting; for simplification, we use a constant learning rate of  $10^{-4}$  during training.

## 4 Model skill

We first evaluate the predictive skill of the various models to the choice of target data. The skill of the models are judged by its ability to reduce mismatches of the divergence of the eddy PV flux, via repeated predictions of smaller patches (here taken with a stride of 2 pixels), with averages taken as necessary. Note that while  $f_{\text{div}}^q(\dots)$  already predicts the divergence of the eddy PV flux, we will take a divergence of the outcome of  $f_{\text{full/eff}}^q(\dots)$  to give the predicted divergence of the eddy PV flux. The normalized mismatch between data and prediction will be judged as

$$\epsilon_{L^2}^q(F_{(\cdot)}^q) = \frac{\|\nabla \cdot \overline{\mathbf{u}'q'} - F_{(\cdot)}^q(\dots)\|_{L^2}^2}{\|\nabla \cdot \overline{\mathbf{u}'q'}\|_{L^2}^2}, \quad (10)$$

where  $F_{(\cdot)}^q$  denotes the divergence of the eddy PV flux from the models  $f_{(\cdot)}^q(\dots)$ , and the  $L^2$  norm is defined as

$$\|g\|_{L^2}^2 = \int_A g^2 \, dA \quad (11)$$

for some scalar field  $g$ . Each ensemble member will make a set of predictions with an associated mismatch, and the associated averages and standard deviations computed to gauge model skill.

We note that the test for skill chosen here is inherently harder and biased *against* the models trained on the eddy PV fluxes (filtered or otherwise), since an extra divergence operation is required in computing the mismatches. The above choice to compare the divergence of the eddy PV flux was taken noting that we want a quantity that is comparable across the three sets of models, and there is a theoretical issue in comparing quantities at the eddy PV flux level (since that requires integrating the prediction of  $F_{\text{div}}^q(\dots)$ , which is then subject to a choice of boundary condition). One could argue whether it is the  $L^2$  mismatches we are ultimately interested in, since we may for example be interested in the patterns of the forcing, rather than the exact locations of the forcing. As a compromise, we consider the Sobolev semi-norms (e.g. Thiffeault, 2012) given by

$$\|g\|_{\dot{H}^p}^2 = \int_A |(-\nabla^2)^p g|^2 \, dA = \sum_{k^2+l^2 \neq 0} (k^2 + l^2)^p |\hat{g}_{k,l}|^2, \quad (12)$$

where  $\hat{g}_{k,l}$  are the Fourier coefficients of  $g$ ,  $(k, l)$  are the respective wavenumbers, and the link between integral and sum follows from Parseval's theorem (e.g. if  $p = 0$  then it is the  $L^2$  norm above when the  $k = l = 0$  mode is included). Sobolev semi-norms with negative  $p$  will weigh the lower wavenumbers (i.e. the larger-scale patterns) more, and in this instance a lower normalized mismatch

$$\epsilon_{\dot{H}^p}^q(F_{(\cdot)}^q) = \frac{\|\nabla \cdot \overline{\mathbf{u}'q'} - F_{(\cdot)}^q(\dots)\|_{\dot{H}^p}^2}{\|\nabla \cdot \overline{\mathbf{u}'q'}\|_{\dot{H}^p}^2} \quad (13)$$

indicates that the mismatches at the large-scales are smaller. Since we are dealing with finite approximations so that  $k^2 + l^2 < \infty$ , we can perform the computation, although the formal definition for the  $\dot{H}^p$  semi-norms is generally for fields with zero mean and on a periodic domain and such that the infinite sum converges. For the work here we will focus on the case of  $p = -1/2$ , sometimes referred to as the mix-norm (e.g. Thiffeault, 2012); conclusions below are qualitatively the same if  $p = -1$  or  $p = -2$  were chosen (not shown).

### 4.1 Models trained on eddy PV fluxes

We first focus on models trained up on the data based on the eddy PV flux  $\overline{\mathbf{u}'q'}$  with the time-mean streamfunction  $\overline{\psi}$  as the input. Fig. 3 shows the predicted divergence of the eddy PV flux  $F_{\text{div/full/eff}}^q(\overline{\psi})$  as an output from one of the model ensemble members. Compared to the target given in Fig. 1(a), the predictions are more smooth with

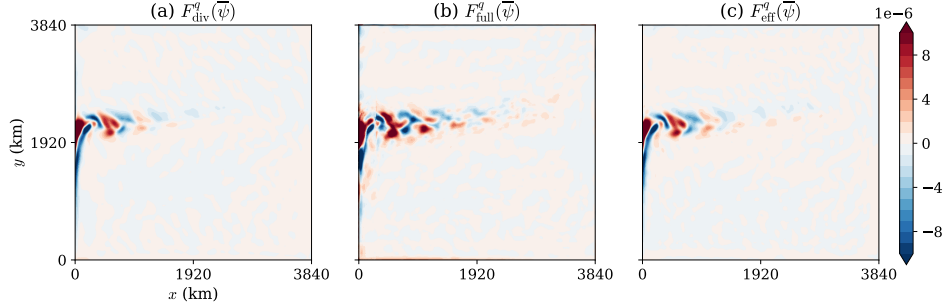


**Figure 3.** Prediction of the divergence of eddy PV flux (units of  $\text{m}^2 \text{s}^{-2}$ ) from one of the ensemble member of models. (a)  $F_{\text{div}}^q(\bar{\psi})$ , (b)  $F_{\text{full}}^q(\bar{\psi})$ , (c)  $F_{\text{eff}}^q(\bar{\psi})$ . The target reference data shown in Fig. 1a.

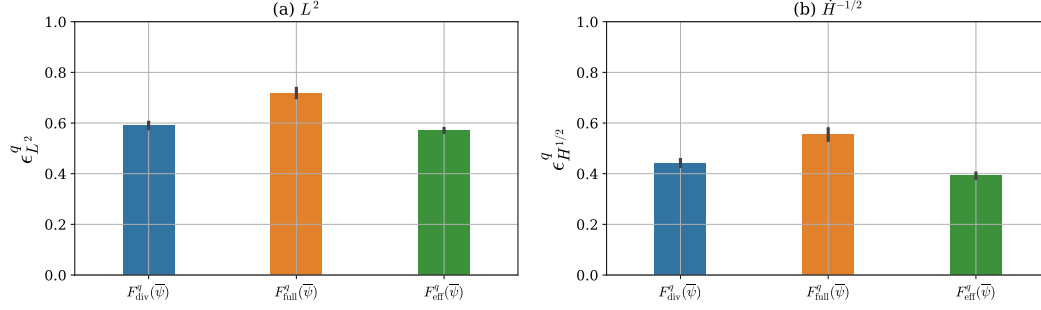
fewer small-scale features, arising from a combination of the fact that CNNs were used, and that our prediction step leads to some averaging of the overlapping regions. Visually, the predictions  $F_{\text{div}}^q(\bar{\psi})$  and  $F_{\text{eff}}^q(\bar{\psi})$  are almost indistinguishable (the latter having a slightly stronger signal downstream of the Western Boundary Current). On the other hand, the prediction  $F_{\text{full}}^q(\bar{\psi})$  shows more fluctuation features than the other two cases. The larger amount of small-scale features in  $F_{\text{full}}^q(\bar{\psi})$  likely arises because the model is predicting the eddy PV flux first, before taking a numerical divergence of the data, so any small fluctuations that arise from the prediction is amplified by the divergence operation. In that regard, the fact that the prediction  $F_{\text{eff}}^q(\bar{\psi})$  is so similar to  $F_{\text{div}}^q(\bar{\psi})$  is rather remarkable.

Fig. 4 shows the more quantitative measure of computing various mismatches in the  $L^2$  norm and the  $\dot{H}^{-1/2}$  semi-norm given in Eq. (11) and (12) respectively. The results show that the models trained upon the filtered eddy PV flux  $-\nabla\Psi_{\text{eff}}^q$  outperforms the models trained upon the full eddy PV flux  $\mathbf{u}'q'$ , and have a comparable or even better performance compared to the models trained up on the divergence of the eddy PV flux  $\nabla \cdot \mathbf{u}'q'$ . The differences in skill are visually obvious between the models trained on the full eddy flux  $\mathbf{u}'q'$  and the filtered eddy flux  $-\nabla\Psi_{\text{eff}}^q$ . The difference between the models trained from the filtered eddy flux  $-\nabla\Psi_{\text{eff}}^q$  and the divergence of the eddy flux  $\nabla \cdot \mathbf{u}'q'$ , while notable in the  $\dot{H}^{-1/2}$  measure, is too close to call in the  $L^2$  measure (e.g. we do not have  $p < 0.05$  using the Student's  $t$ -test (Student, 1908) under the null hypothesis that the means of  $F_{\text{div}}^q(\bar{\psi})$  and  $F_{\text{eff}}^q(\bar{\psi})$  are the same).

The results here lend support to our expectation that the presence of rotational fluxes contaminate and degrade the accuracy of a trained up model, and that the eddy force function provides an viable alternative for use in machine learning approaches that addresses the problem of dynamically inert rotational fluxes, leading to at least comparable performance from a skill point of view (and some evidence to suggest it might be better, although that is dependent on the choice of metric). The observation that  $F_{\text{eff}}^q(\bar{\psi})$  is comparable to  $F_{\text{div}}^q(\bar{\psi})$  is all the more remarkable when we note that tests based on the models' ability in reproducing the divergence of the eddy flux is intrinsically harder and biased against models trained on  $-\nabla\Psi_{\text{eff}}^q$ , since an additional divergence operation that is expected to amplify errors is required to produce  $F_{\text{eff}}^q(\bar{\psi})$ .

## 4.2 Other choice of eddy fluxes and inputs

By the linearity assumption in deriving the eddy force function and the definition of PV, analogous eddy force functions for momentum and buoyancy may be defined by



**Figure 4.** Ensemble average and quartiles of the mismatch as measured by the normalized (a)  $L^2$  norm (b)  $\dot{H}^{-1/2}$  semi-norm, given by Eq. (10) and (13) respectively, for the models predicting the divergence of the eddy PV flux (Fig. 1a). Blue denotes models trained on the divergence of the eddy fluxes, orange denotes models trained on the full eddy fluxes, and green denotes models trained on the filtered eddy fluxes.

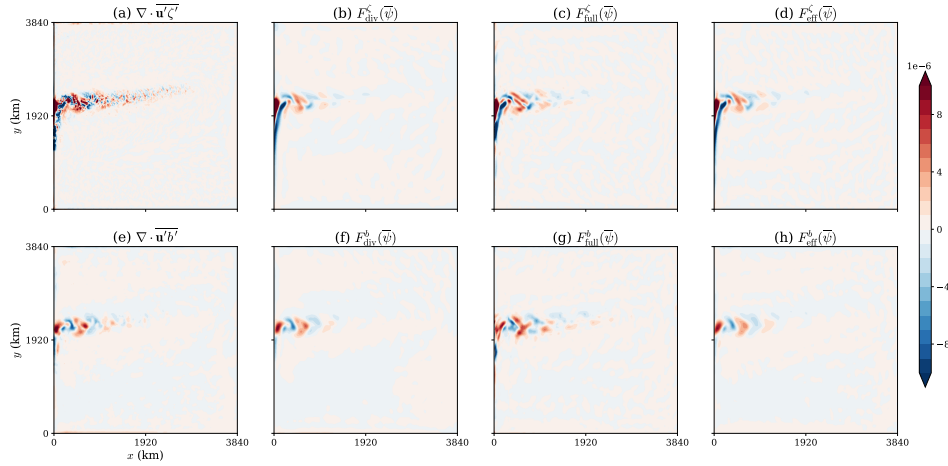


**Figure 5.** Target data and predictions associated with (top row) eddy relative vorticity flux (related to the Reynolds stress, units of  $\text{m s}^{-2}$ ) and (bottom row) eddy buoyancy flux (related to the form stress, units also of  $\text{m s}^{-2}$  taking into account of the extra factors). Showing (a, e) the divergence of the time-averaged eddy relative vorticity and buoyancy flux, and a sample (b, f)  $F_{\text{div}}^{\zeta/b}(\bar{\psi})$ , (c, g)  $F_{\text{full}}^{\zeta/b}(\bar{\psi})$ , (d, h)  $F_{\text{eff}}^{\zeta/b}(\bar{\psi})$  from one of the ensemble members.

a similar decomposition but using the eddy relative vorticity flux  $\overline{\mathbf{u}'\zeta'}$  (related to the Reynolds stress via the Taylor identity) and  $\overline{\mathbf{u}'b'}$  (related to the form stress). Following the notation outline above, Fig. 5 show the target data  $\nabla \cdot \overline{\mathbf{u}'\zeta'}$  and  $\nabla \cdot \overline{\mathbf{u}'b'}$ , and the analogous predictions of the divergence of the fluxes denoted by  $F_{\text{div/full/eff}}^{\zeta/b}(\bar{\psi})$ .

For the models trained on the data relating to the eddy PV flux shown in Fig. 1, the predictions are more smooth than the diagnosed target data, and is particularly noticeable for prediction of the divergence of the eddy relative vorticity flux in Fig. 5(b, c, d). For the eddy buoyancy case, the diagnosed target data is already relatively smooth. We note that, visually,  $F_{\text{full}}^b(\bar{\psi})$  in Fig. 5(g) seems to be possess extra features particularly in the downstream region, while  $F_{\text{eff}}^b(\bar{\psi})$  and  $F_{\text{div}}^b(\bar{\psi})$  in Fig. 5(f, h) seems to be captur-

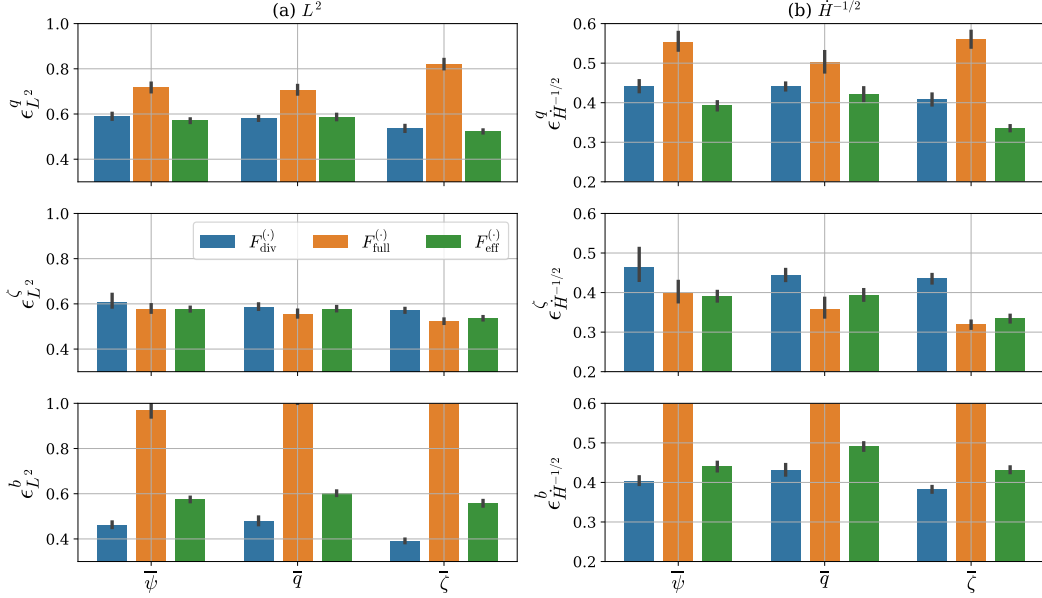


**Figure 6.** Ensemble average and quartiles of the normalized (a)  $L^2$  norm (b)  $\dot{H}^{-1/2}$  semi-norm, given by Eq. (10) and (13) respectively, for the models predicting the divergence of the eddy (rows) PV flux, relative vorticity (cf. momentum) flux, and buoyancy flux, over various choices of inputs. Blue denotes models trained on the divergence of the eddy fluxes, orange denotes models trained on the full eddy fluxes, and green denotes models trained on the filtered eddy fluxes. Top row is identical to Fig. 4. The mismatches in  $F_{\text{full}}^b(\bar{q})$  and  $F_{\text{full}}^b(\bar{\zeta})$  are out of range of panel, with values around 1.0 and 1.5 respectively.

ing the patterns in the target data well, with some visual hints that the prediction from  $F_{\text{div}}^b(\bar{\psi})$  has slightly sharper features.

For a more quantitative measure, we show in Fig. 6 the  $L^2$  and  $\dot{H}^{-1/2}$  mismatches in  $F_{\text{div}/\text{full}/\text{eff}}^{q/\zeta/b}(\bar{\psi}/\bar{q}/\bar{\zeta})$ , totaling the  $3^3 = 27$  possible combinations. The conclusions over all these possible choices are largely what was drawn from before but with minor differences. The models trained up on the filtered eddy fluxes outperform those trained upon the full eddy fluxes (except for the case of eddy relative vorticity fluxes), and are comparable or better than models trained on the divergence of the flux (except in the case of the eddy buoyancy fluxes).

Noting that eddy PV fluxes have contributions from the eddy buoyancy as well as eddy relative vorticity fluxes, it is curious that while models trained on the filtered eddy fluxes compared with models trained on the divergence of the flux appear to perform worse for the eddy buoyancy flux (bottom row of Fig. 6), but has reasonable performance in the eddy relative vorticity flux case (middle row of Fig. 6) such that, together, the resulting skill in the eddy PV flux (top row of Fig. 6) still remains comparable (and possibly slightly better in the  $\dot{H}^{-1/2}$  semi-norm, indicating better matching in terms of large-scale patterns). One possible explanation for the degradation in performance for eddy buoyancy fluxes is that  $\nabla \cdot \mathbf{u}'\mathbf{b}'$  is already relatively smooth and larger-scale (Fig. 5e), which might be favorable for direct use as training data. On the other hand, the eddy relative vorticity fluxes are inherently smaller-scale (Fig. 5a), and the presence of small-scale fluctuation might be unfavorable for direct use as training data, but does not affect models trained on the filtered fluxes as such since the training data is by definition

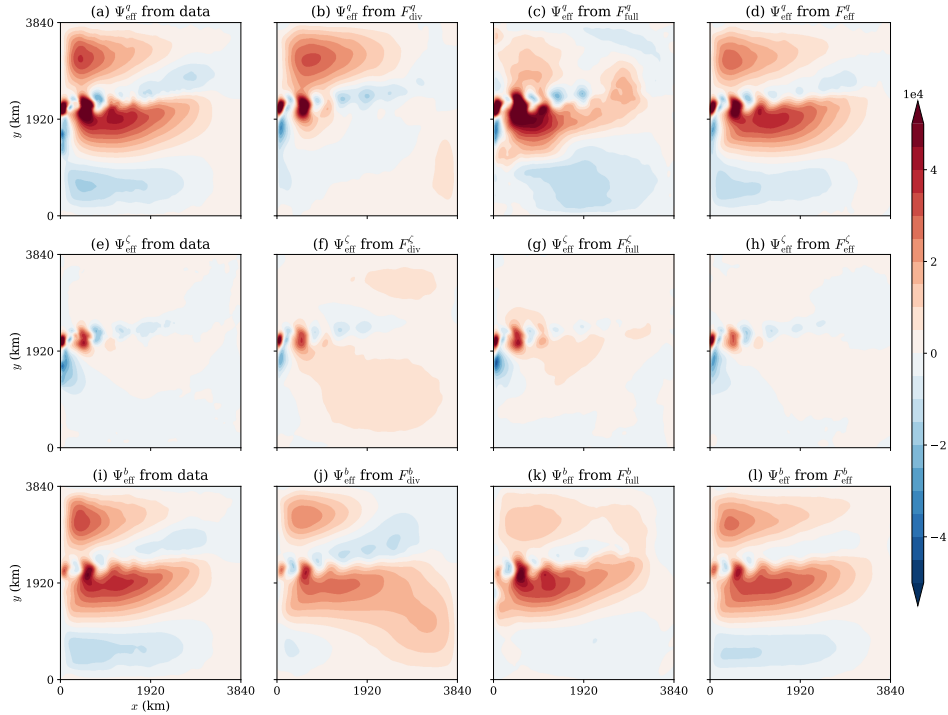


**Figure 7.** (a, e, i) Target eddy force functions  $\Psi_{\text{eff}}^{q/\zeta/b}$ , and eddy force functions associated with prediction from (b, f, j) divergence of the eddy PV, relative vorticity and buoyancy fluxes, (c, g, k) full eddy PV, relative vorticity and buoyancy fluxes, and (d, h, l) filtered eddy PV, relative vorticity and buoyancy fluxes, from one of the ensemble members. All data shown here are in units of  $\text{m}^2 \text{s}^{-2}$ .

more smooth. The performance of models based on the full eddy relative vorticity fluxes is somewhat surprising, but may be to do with the smaller component of the rotational fluxes: examining the decomposition into divergent and rotational parts via the eddy force function (cf. Fig. 1b, c, e, f, not shown) it is found that the divergent component is smaller by about a factor of 2 in the eddy relative vorticity flux, but a factor of 10 in the eddy buoyancy and PV flux. The results seem to suggest that the main benefits of filtering dynamically inert rotational fluxes would be in the eddy buoyancy and PV.

For completeness, we show in Fig. 7 the analogous eddy force functions associated with the predictions from the trained models from one of the ensemble members (although observations detailed here are robust upon examining the outputs from other members); note the appropriate mismatches would be closely related to the  $\dot{H}^{-2}$  semi-norm as defined in Eq. (12), but with a difference in the boundary conditions. The predictions from models trained on the filtered eddy fluxes (panels d, h, l) have patterns that are largely aligned with the diagnosed eddy force functions from the data (panels a, e, i) up to minor discrepancies (e.g. downstream patterns in panel d compared to panel a, and panel l compared to panel i). The predictions from models trained on the full eddy fluxes (panels c, g, k) show similar patterns although with somewhat more mismatches, particularly in the PV and buoyancy eddy force functions. By contrast, the predictions from the divergence of the eddy fluxes (panels b, f, j) show large-scale disagreements in all three variables, the mismatches being visually the gravest in the PV and buoyancy variables. Given that the eddy force function encodes the dynamically active eddy fluxes, and has an interpretation that  $\nabla\Psi_{\text{eff}}\cdot\nabla\psi$  encodes the sign of energy exchange between the mean and

eddy component (Maddison et al., 2015), the finding here suggests the predictions from models trained on the divergence of the eddy fluxes are very likely representing erroneous energy transfers, particularly for processes associated with eddy buoyancy fluxes.

## 5 Model robustness

The above observations of model skill and its sensitivity to small-scale fluctuations brings into question the issue of robustness particularly for the models trained on the divergence of the eddy fluxes. To explore the sensitivity of skill to noise in the data, we consider a set of experiments where we add noise  $\eta(x, y)$  to the data at the *training* stage, and judge the models' performance on its ability in predicting the target data without noise. To make sure we are comparing models in a consistent manner, we add an appropriately scaled Gaussian distributed noise  $\eta(x, y)$  to the eddy fluxes  $(\overline{\mathbf{u}'q'}, \overline{\mathbf{u}'\zeta'}, \overline{\mathbf{u}'b'})$ , from which we compute the divergence of the eddy flux as well as the eddy force function from the noisy data, and train up the models using the procedure outlined above. In that sense the whole set of models are exposed to the *same* choice of noise, since 1 unit of noise at the divergence level is not necessarily the same as 1 unit of noise at the streamfunction level. The noise level here is measured in units of the standard deviation of the eddy flux data. The hypothesis is that the models trained on the filtered eddy fluxes are more robust than those trained on the divergence of the eddy fluxes, and able to maintain model skill with increased levels of noise.

A note to make here is that the stochastic noise  $\eta(x, y)$  in this regard is formally non-differentiable in space, so that the divergence operation on it is not well-defined. In terms of numerical implementation, however, the random numbers sampled from the appropriately scaled Gaussian distribution are the nodal values of the finite element mesh used in FEniCS, and there is a projection onto a linear basis, so that a derivative operation on the projected  $\eta(x, y)$  is allowed within FEniCS, though the operation may be numerically sensitive. An approach we considered is filtering the noise field. We consider solving for some  $\tilde{\eta}(x, y)$  satisfying

$$(1 - L^2 \nabla^2)^2 \tilde{\eta} = \eta \quad (14)$$

with no-flux boundary conditions, and it is the resulting  $\tilde{\eta}(x, y)$  that is added to the training data. The resulting  $\tilde{\eta}$  is by construction differentiable at least once so that a divergence is well-defined. For the operator  $(1 - L^2 \nabla^2)^2$ , the associated Green's function has a characteristic length-scale  $L$  that can be interpreted as a filtering length-scale where the radial spectral power density decreases significantly after  $L$  (closely related to the Matérn auto-covariance, e.g. Whittle, 1963; Lindgren et al., 2018). Note that 'noise level' here refers to the magnitude of  $\eta(x, y)$ , and that  $\max |\tilde{\eta}(x, y)| < \max |\eta(x, y)|$  by construction.

The  $L^2$  and  $\dot{H}^{-1/2}$  mismatches of  $F_{\text{div/full/eff}}^{q/\zeta/b}(\bar{\psi})$  to the data as a function of noise level for the ensemble of models is shown in Fig. 8, and consistently we find that the models trained up on the eddy force function out-perform the models trained upon the divergence of the eddy flux. The former shows a relative insensitivity to noise level, while the latter shows a rapid degradation in skill with noise level. It would seem that the use of eddy force function data alleviates the sensitivity to small-fluctuations in data, at least in the present measure and approach.

The reduced sensitivity to noise might have been anticipated, since the eddy force function is a result of an elliptic solve of a Poisson equation, where the noisy data is acted upon by an inverse Laplacian operator that leads to substantial smoothing. We would however argue that the relative insensitivity to noise is somewhat surprising, since there is no guarantee the presence of even reduced fluctuations at the streamfunction level would stay small after spatial derivatives operations, since we are using the divergence of the eddy flux as the target for the measure of skill. While one could also argue that the present

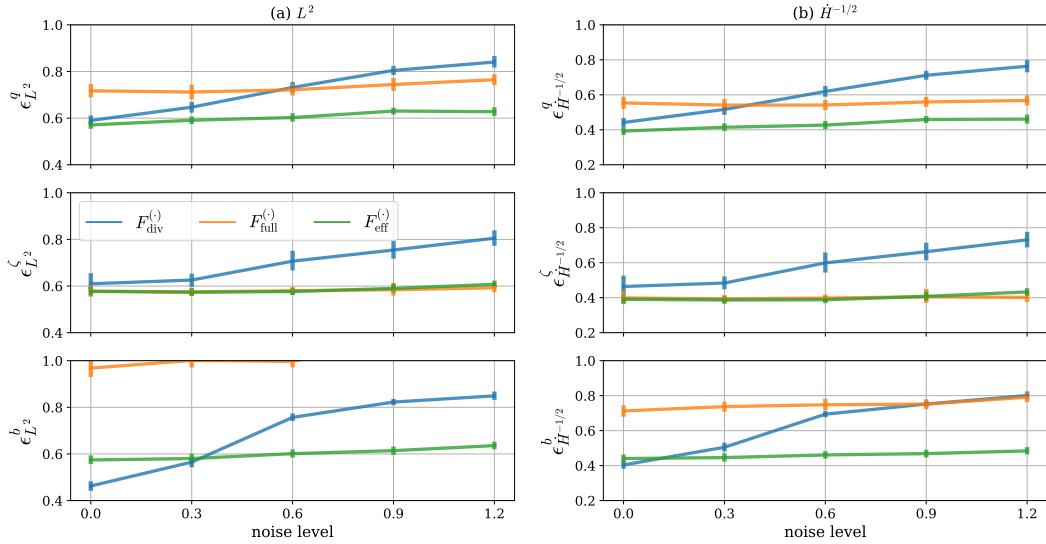


**Figure 8.** Ensemble average and quartiles of the normalized (a)  $L^2$  norm (b)  $\dot{H}^{-1/2}$  semi-norm, given by Eq. (10) and (13) respectively, for the models predicting the divergence of the eddy (rows) PV flux, relative vorticity (cf. momentum) flux, and buoyancy flux as a function of noise level (in units of standard deviation of the training data), for models using the time-mean streamfunction  $\bar{\psi}$  as the input. Blue denotes models trained on the divergence of the eddy fluxes, orange denotes models trained on the full eddy fluxes, and green denotes models trained on the filtered eddy fluxes.

robustness test is inherently a hard test for models trained upon the divergence of the eddy flux, we argue the conclusions are robust regardless of whether the noise is added at the flux, divergence of flux or streamfunction level. In fact, the use of the divergence of a flux as training data *is* likely the cause for sensitivity to noise: a inherently small-scale field is sensitive to the presence of noise in data, so is likely going to lead to issues with robustness.

The conclusions in the above are qualitatively robust for different choices of the filtering length-scale  $L$ : with reduced  $L$ , the degradation of skill in models trained on the divergence of the eddy fluxes is more rapid with noise level, but the skill of models trained on the filtered eddy fluxes is still relatively insensitive to noise level, and consistently more skillful than models trained on the divergence of the eddy fluxes. The conclusions are also robust for different choices of inputs ( $\bar{\zeta}$  and  $\bar{q}$ ), and with sample calculations employing other choices of smoothing, coarse-graining (e.g., Aluie, 2019) or filtering (e.g., Grooms et al., 2021) of the noise field  $\eta(x, y)$ .

## 6 Conclusions and outlooks

Data-driven methods are increasingly being employed in problems of Earth System Modeling, and there is no doubt that such methods provide a powerful tool that can in principle be leveraged to not only improve our modeling efforts, but also deepen our underlying understanding of the problems. Most works in the literature thus far has focused on demonstrating the efficacy of the machine-learning methods and algorithms. Here we take a complimentary line of investigation in considering the choice and quality of data itself being fed into the algorithms, for a case where we have some theoretical understanding to inform our choice of data. While one could argue this is not en-

tirely necessary if we just want something that ‘works’ in the relevant metric(s) for the problem, we argue it is incredibly useful and if not necessary if we want to be leveraging data-driven methods to learn about the underlying physical problems, and/or have beyond ‘black-box’ models. Furthermore, the choice of data can in principle improve the training and/or the performance of the data-driven models themselves, so there is a need for such an investigation into data quality and information content.

For this work we focused on the problem of eddy-mean interaction in rotating stratified turbulence in the presence of boundaries, relevant to the modeling and parameterization of ocean dynamics. In such systems it is known that the large-scale mean affects and is affected by the small-scale eddy fluxes, and while we might want to leverage data-driven methods to learn about the relationship between the mean and the eddy fluxes, it is known that in the presence of boundaries the eddy feedback onto the mean is invariant up to a rotational gauge (e.g. J. C. Marshall & Shutts, 1981; Fox-Kemper et al., 2003; Eden et al., 2007). In practice the dynamically inert component could be quite large (e.g., Griesel et al., 2009, , Fig. 1 here), and its presence might be expected to contaminate diagnoses and/or performance of data-driven models. One possible way round is to train models based on its divergence (e.g., Bolton & Zanna, 2019; Zanna & Bolton, 2021). Here we propose that data with the dynamically inert eddy fluxes filtered out could be used instead. The approach outlined here we argued here may have the advantage in that the resulting field is inherently larger-scale, which would help with model training and sensitivity, and be theoretically more appropriate to use if we want to learn about the underlying physics of the problem, because we do not expect the operations to be commutative (i.e. given the nonlinearity, learning from the divergence is not guaranteed to be the same as the divergence of the learned result).

The experimental approach here largely follows that of Bolton and Zanna (2019), where we diagnose the various data from a quasi-geostrophic double gyre model to train the model, and compare the model’s performance in its prediction. For filtering the eddy flux we employ the eddy force function (e.g. D. P. Marshall & Pillar, 2011; Maddison et al., 2015; Mak et al., 2016), which in the present simply connected quasi-geostrophic system is provably optimal in the  $L^2$  norm (and thus unique; see Appendix of Maddison et al., 2015). We made the choice here to measure a model’s skill in being able to reproduce the divergence of the eddy fluxes over an ensemble of models with 20 members and over a variety of input choices. The findings here are that the models trained on the eddy force function are (a) more skillful than those trained on the full eddy flux (except for the relative vorticity eddy fluxes), (b) at least comparable in skill than models trained on the divergence of the eddy fluxes (except for the buoyancy eddy fluxes), and on occasion better, especially in the  $\dot{H}^{-1/2}$  semi-norm compared to the  $L^2$  norm, where the former biases matching of the large-scale patterns of the resulting predictions, and (c) more robust in that the models are less sensitive to noise in the training data. The first finding is perhaps not unexpected. The latter two findings we argue are not entirely obvious, given divergence operations acting at various steps. For example, sample calculations where a model is trained on the eddy force function directly (and then taking a Laplacian to obtain a prediction of the divergence of eddy flux) leads to larger mismatches, which we attribute to the fact that any mismatches in the predicted eddy force function is significantly amplified by the two derivative operations. With that in mind, the fact that models trained on the filtered flux reported here leveraging the eddy force function as a way to filter data leads to models with comparable or better skill and superior robustness is a non-trivial result.

Exceptions to the above conclusions are that models trained on the divergence of the eddy buoyancy flux are more skillful (bottom row of Fig. 6), and models trained on the eddy relative vorticity flux appear comparable whether the rotational component is filtered out or not (middle row of Fig. 6). The former might be justified in that the eddy buoyancy flux is already relatively smooth and somewhat larger-scale, so that training

on its divergence is not such an issue; however, we also note that the buoyancy eddy force functions associated with the predictions of model trained on the divergence of the eddy buoyancy flux seems to perform the worse (bottom of Fig. 7), implying erroneous predictions of eddy energy pathways. The latter behavior is possibly to do with the observation that the dynamically inert rotational component is comparable to the dynamically active divergent component in the eddy relative vorticity flux (as opposed to the rotational component being a factor of ten smaller in the eddy PV and buoyancy flux; see Fig. 1*b, c, e, d* for eddy PV flux), so the effect of filtering is somewhat marginal. One saving grace is that, in the quasi-geostrophic system, the potential vorticity (with contributions from relative vorticity and buoyancy) is the master variable, and that while models trained up on the relative vorticity or buoyancy fluxes perform better separately, the models trained up on the eddy force function has skill and robustness in the master variable. We note that the conclusions reported here appear to be robust even if we use data with only some of the rotational component filtered out in sample calculations (e.g., solving for  $\psi$  in Eq. 6 with no normal flux boundary conditions, not shown), although we lose a little bit of skill and the physical interpretation associated with the eddy force function.

One thing we caution here is drawing a one-to-one comparison of the present work with that of Bolton and Zanna (2019) and Zanna and Bolton (2021). While it is true those works utilize a similar model, experimental procedure and data, the main theoretical difference is that the choice of average is different: their work utilizes a spatial average, and the eddy flux data there is defined as the difference between the filtered divergence and the divergence of the filtered field (if making an assumption of the zero divergence condition on the resulting velocities). Here we utilize a *time* average, which is in line with the definition of the eddy force function in Maddison et al. (2015), which requires a Reynolds average. While we have not attempted a similar investigation in the case of spatial averaging, it is not implausible that there is an analogous object to the eddy force function when a spatial average is employed, or that a simple Helmholtz-type decomposition could yield the desired filtering of the dynamically inert rotational component, but is beyond the scope of the present investigation.

Because of the choice of time average, we have limited data in time, and one could wonder whether our conclusions are simply to do with the limited data availability. This is unlikely the case: we also carried out an analogous investigation with rolling time averages as well as *ensemble* averages (not shown), and the conclusions drawn from those results are essentially identical to those here. This is perhaps not surprising noting that the rolling time averages for a long enough window and the ensemble averages shown no strong deviations from each other, but we note this is likely only true for a sufficiently simple system with no strong evidence of internal modes of variability, such as the one employed here.

The main intention of the present work is to demonstrate that not all data choices are equal when fed to data-driven methods, and it is not always advisable throwing all the available data at the machine and trust that the machine will figure out what to do with it (although one could argue that might reduce the inherent biases). For the case of rotating stratified turbulence, the eddy force function is potentially a useful quantity if we aim to leverage data-drive methods for model skill or for learning about the underlying physics of the problem, given the various theoretical expectations highlighted in this work. Other choices may be possible: in a periodic domain often used in rotating turbulence studies (e.g., Frezat et al., 2022; Ross et al., 2023), a standard Helmholtz decomposition could be used to solve for the divergent component, although the eddy force could still be used for physical interpretation. We note that while skill in reproducing eddy forcing is one target, we have not examined here on the ability of the model to reproduce the mean state, and the present procedure might be termed an ‘offline’ approach. Learning ‘online’ (e.g., Frezat et al., 2022) may be more appropriate for param-

eterization purposes to improve on the mean response, and it would be of interest to see whether filtering of the eddy flux as discussed here would confer any benefits to model learning.

The present work also highlights questions relating to information content of data. While quantifying absolute data information content is likely quite difficult, it should be at least possible to compute a relative measure, even if empirically. Preliminary investigation indicates that as the amount of data exposed to the machine learning algorithm is reduced, the accuracy of models trained upon the full eddy flux or the divergence of the eddy flux degrades much faster than models trained upon the eddy force function. One might ask an analogous question of the input data. The work of Bolton and Zanna (2019) suggests for example that training with data from regions with higher eddy kinetic energy leads to better model performance in terms of accuracy, suggestive of higher information content in said region. Within the present experimental framework, instead of training using all the data and performing a random sampling of the sub-regions considered in this work, we could consider instead not using all the data, and perform training based on a biased sampling that favor regions with higher eddy energy content, with the hypothesis that the latter case leads to models with higher accuracy from a statistical point of view. Further, we could investigate the case of multiple inputs, where we hypothesize that eddy energy and a mean state variable as inputs might lead to improved performance compared to say two mean state variables: in the current quasi-geostrophic setting, the mean state variables are functionally related to each other, possibly leading to redundant information, while the eddy energy might be dependent on the mean state, but is capturing eddy statistics instead and providing complementary information. This investigation is ongoing and will be reported elsewhere in due course.

## Data Availability Statement

This work utilizes FEniCS (2019.1.0) that is available as a Python package. The source code for the model (`qgm2`, from James Maddison), sample model data and scripts used for generating the plots in this article from the processed data are available through <http://dx.doi.org/10.5281/zenodo.8072817>.

## Acknowledgments

This research was funded by both RGC General Research Fund 16304021 and the Center for Ocean Research in Hong Kong and Macau, a joint research center between the Qingdao National Laboratory for Marine Science and Technology and Hong Kong University of Science and Technology. We thank James Maddison and Liying Yeow for various scientific and technical comments in relation to the present investigation, and the former for providing the `qgm2` code for use in the present work.

## References

- Alnæs, M. S., Logg, A., Ølgaard, K. B., Rognes, M. E., & Wells, G. N. (2014). Unified Form Language: A domain-specific language for weak formulations of partial differential equations. *ACM Trans. Math. Softw.*, *40*, 9:1–9:37.
- Aluie, H. (2019). Convolutions on the sphere: Commutation with differential operators. *GEM: Int. J. Geomath.*, *10*, 1–31. doi: 10.1007/s13137-019-0123-9
- Andersson, T. R., Hosking, J. S., Pérez-Ortiz, M., Paige, B., A. Elliott, C. R., Law, S., . . . Shuckburgh, E. (2021). Seasonal Arctic sea ice forecasting with probabilistic deep learning. *Nat. Commun.*, *12*, 5124. doi: 10.1038/s41467-021-25257-4
- Barnes, E. A., Barnes, R. J., Martin, Z. K., & Rader, J. K. (2022). This looks like that there: Interpretable neural networks for image tasks when

- location matters. *Artif. Intell. Earth Syst.*, 1(3), e220001. doi: 10.1175/AIES-D-22-0001.1
- Berloff, P. (2005). On dynamically consistent eddy fluxes. *Dyn. Atmos. Ocean.*, 38, 123–146.
- Besombes, C., Pannekoucke, O., Lapeyre, C., Sanderson, B., & Thual, O. (2021). Producing realistic climate data with generative adversarial networks. *Nonlinear Process Geophys.*, 28(3), 347–370. doi: 10.5194/npg-28-347-2021
- Beucler, T., Pritchard, M., Rasp, S., Ott, J., Baldi, P., & Gentine, P. (2021). Enforcing analytic constraints in neural networks emulating physical systems. *Phys. Rev. Lett.*, 126, 098302. doi: 10.1103/PhysRevLett.126.098302
- Bolibar, J., Rabatel, A., Gouttevin, I., Galiez, C., Condom, T., & Sauquet, E. (2020). Deep learning applied to glacier evolution modelling. *Cryosphere*, 14(2), 565–584. doi: 10.5194/tc-14-565-2020
- Bolton, T., & Zanna, L. (2019). Applications of deep learning to ocean data inference and sub-grid parameterisation. *J. Adv. Model. Earth Syst.*, 11, 376–399. doi: 10.1029/2018MS001472
- Brenowitz, N. D., Beucler, T., Pritchard, M., & Bretherton, C. S. (2020). Interpreting and stabilizing machine-learning parametrizations of convection. *J. Atmos. Sci.*, 77, 4357–4375. doi: 10.1175/JAS-D-20-0082.1
- Brenowitz, N. D., & Bretherton, C. S. (2019). Spatially extended tests of a neural network parametrization trained by coarse-graining. *J. Adv. Model. Earth Syst.*, 11, 2728–2744. doi: 10.1029/2019MS001711
- Camps-Valls, G., Gerhardus, A., Ninad, U., Varando, G., Martius, G., Balaguer-Ballester, E., ... Runge, J. (2023). *Discovering Causal Relations and Equations from Data*.
- Clare, M. C. A., Sonnewald, M., Lguensat, R., Deshayes, J., & Balaji, V. (2022). Explainable Artificial Intelligence for Bayesian neural networks: Toward trustworthy predictions of ocean dynamics. *J. Adv. Model. Earth Syst.*, 14(11), e2022MS003162. doi: 10.1029/2022MS003162
- Connolly, C., Barnes, E. A., Hassanzadeh, P., & Pritchard, M. (2023). Using neural networks to learn the Jet Stream forced response from natural variability. *Artif. Intell. Earth Syst.*, 2, e220094. doi: 10.1175/AIES-D-22-0094.1
- Eden, C., Greatbatch, R. J., & Olbers, D. (2007). Interpreting eddy fluxes. *J. Phys. Oceanogr.*, 37, 1282–1296.
- Fox-Kemper, B., Ferrari, R., & Pedlosky, J. (2003). On the indeterminacy of rotational and divergent eddy fluxes. *J. Phys. Oceanogr.*, 33, 478–483.
- Frezat, H., Le Sommer, J., Fablet, R., Balarac, G., & Lguensat, R. (2022). A posteriori learning for quasi-geostrophic turbulence parametrization. *J. Adv. Model. Earth Syst.*, 14(11), e2022MS003124. doi: 10.1029/2022MS003124
- Goodfellow, I., Bengio, Y., & Courville, A. (2016). *Deep learning*. MIT Press. (<http://www.deeplearningbook.org>)
- Green, J. S. A. (1970). Transfer properties of the large-scale eddies and the general circulation of the atmosphere. *Q. J. Roy. Met. Soc.*, 96, 157–185.
- Griesel, A., Gille, S. T., Sprintall, J., McClean, J. L., & Maltrud, M. E. (2009). Assessing eddy heat flux and its parameterization: A wavenumber perspective from a  $1/10^\circ$  ocean simulation. *Ocean Modell.*, 29, 248–260.
- Grooms, I., Loose, N., Abernathey, R., Steinberg, J. M., Bachman, S. D., Marques, G., ... Yankovsky, E. (2021). Diffusion-based smoothers for spatial filtering of gridded geophysical data. *J. Adv. Model. Earth Syst.*, 13, e2021MS002552. doi: 10.1029/2021MS002552
- Guan, Y., Subel, A., Chattopadhyay, A., & Hassanzadeh, P. (2023). Learning physics-constrained subgrid-scale closures in the small-data regime for stable and accurate LES. *Physica D*, 443, 133568. doi: 10.1016/j.physd.2022.133568
- Guillaumin, A. P., & Zanna, L. (2021). Stochastic-deep learning parameterization of ocean momentum forcing. *J. Adv. Model. Earth Syst.*, 13, e2021MS002534.

doi: 10.1029/2021MS002534

- Irrgang, C., Boers, N., Sonnewald, M., Barnes, E. A., Kadow, C., Staneva, J., & Saynisch-Wagner, J. (2021). Towards neural Earth system modelling by integrating artificial intelligence in Earth system science. *Nat. Mach. Intell.*, *3*, 667–674. doi: 10.1038/s42256-021-00374-3
- Jones, D. C., Holt, H. J., Meijers, A. J. S., & Shuckburgh, E. (2019). Unsupervised clustering of Southern Ocean Argo float temperature profiles. *J. Geophys. Res. Oceans*, *124*(1), 390–402. doi: 10.1029/2018JC014629
- Karabasov, S. A., Berloff, P. S., & Goloviznin, V. M. (2009). CABARET in the ocean gyres. *Ocean Modell.*, *30*, 155–168.
- Kashinath, K., Mustafa, M., Albert, A., Wu, J., Jiang, C., Esmailzadeh, S., . . . Prabhat (2021). Physics-informed machine learning: case studies for weather and climate modelling. *Philos. Trans. Royal Soc. A*, *379*(2194), 20200093. doi: 10.1098/rsta.2020.0093
- Kingma, D. P., & Ba, J. (2015). Adam: A method for stochastic optimization. In Y. Bengio & Y. LeCun (Eds.), *Iclr (poster)*.
- Lindgren, F., Rue, H., & Lindström, J. (2018). An explicit link between Gaussian fields and Gaussian Markov random fields: The stochastic partial differential equation approach. *J. R. Stat. Soc. Series B Stat. Methodol.*, *73*, 423–498. doi: 10.1111/j.1467-9868.2011.00777.x
- Logg, A., Mardal, K. A., & Wells, G. N. (2012). *Automated Solution of Differential Equations by the Finite Element Method*. Springer.
- Logg, A., & Wells, G. N. (2010). DOLFIN: Automated finite element computing. *ACM Trans. Math. Softw.*, *37*, 20:1–20:28.
- Lopez-Gomez, I., Christopoulos, C., Langeland Ervik, H. L., Dunbar, O. R. A., Cohen, Y., & Schneider, T. (2022). Training physics-based machine-learning parameterizations with gradient-free ensemble Kalman methods. *J. Adv. Model. Earth Syst.*, *14*(8), e2022MS003105. doi: 10.1029/2022MS003105
- Maddison, J. R., & Marshall, D. P. (2013). The Eliassen–Palm flux tensor. *J. Fluid Mech.*, *729*, 69–102. doi: 10.1017/jfm.2013.259
- Maddison, J. R., Marshall, D. P., & Shipton, J. (2015). On the dynamical influence of ocean eddy potential vorticity fluxes. *Ocean Modell.*, *92*, 169–182.
- Mak, J., Maddison, J. R., & Marshall, D. P. (2016). A new gauge-invariant method for diagnosing eddy diffusivities. *Ocean Modell.*, *104*, 252–268. doi: 10.1016/j.ocemod.2016.06.006
- Marshall, D. P., Maddison, J. R., & Berloff, P. S. (2012). A framework for parameterizing eddy potential vorticity fluxes. *J. Phys. Oceanogr.*, *42*, 539–557. doi: 10.1175/JPO-D-11-048.1
- Marshall, D. P., & Pillar, H. R. (2011). Momentum balance of the wind-driven and meridional overturning circulation. *J. Phys. Oceanogr.*, *41*, 960–978.
- Marshall, J. C. (1981). On the parameterization of geostrophic eddies in the ocean. *J. Phys. Oceanogr.*, *11*, 257–271.
- Marshall, J. C., & Shutts, G. J. (1981). A note on rotational and divergent eddy fluxes. *J. Phys. Oceanogr.*, *11*, 1677–1680. doi: 10.1175/1520-0485(1981)011(1677:ANORAD)2.0.CO;2
- Mooers, G., Pritchard, M., Beucler, T., Ott, J., Yacalis, G., Baldi, P., & Gentine, P. (2021). Assessing the potential of deep learning for emulating cloud superparameterization in climate models with real-geography boundary conditions. *J. Adv. Model. Earth Syst.*, *13*, e2020MS002385. doi: 10.1002/2020MS002385
- Paszke, A., Gross, S., Massa, F., Lerer, A., Bradbury, J., Chanan, G., . . . Chintala, S. (2019). Pytorch: An imperative style, high-performance deep learning library. In H. Wallach, H. Larochelle, A. Beygelzimer, F. d'Alché-Buc, E. Fox, & R. Garnett (Eds.), *Advances in neural information processing systems* (Vol. 32). Curran Associates, Inc.

- Reichstein, M., Camps-Valls, G., Stevens, B., Jung, M., Denzler, J., Carvalhais, N., & Prabhat. (2019). Deep learning and process understanding for data-driven Earth system science. *Nature*, *566*, 195–204. doi: 10.1038/s41586-019-0912-1
- Rhines, P. B., & Young, W. R. (1982). Homogenization of potential vorticity in planetary gyres. *J. Fluid Mech.*, *122*, 347–367.
- Ross, A., Li, Z., Perezhogin, P., Fernandez-Granda, C., & Zanna, L. (2023). Benchmarking of machine learning ocean subgrid parameterizations in an idealized model. *J. Adv. Model. Earth. Syst.*, *15*(1), e2022MS003258. doi: 10.1029/2022MS003258
- Sonnewald, M., & Lguensat, R. (2021). Revealing the impact of global heating on North Atlantic circulation using transparent machine learning. *J. Adv. Model. Earth. Syst.*, *13*(8), e2021MS002496. doi: 10.1029/2021MS002496
- Sonnewald, M., Lguensat, R., Jones, D. C., Dueben, P. D., Brajard, J., & Balaji, V. (2021). Bridging observations, theory and numerical simulation of the ocean using machine learning. *Environ. Res. Lett.*, *16*(7), 073008. doi: 10.1088/1748-9326/ac0eb0
- Sonnewald, M., Reeves, K. A., & Lguensat, R. (2023). A Southern Ocean supergyre as a unifying dynamical framework identified by physics-informed machine learning. *Commun. Earth Environ.*, *4*, 153. doi: 10.1038/s43247-023-00793-7
- Sonnewald, M., Wunsch, C., & Heimbach, P. (2019). Unsupervised learning reveals geography of global ocean dynamical regions. *Earth Space Sci.*, *6*(5), 784–794. doi: 10.1029/2018EA000519
- Student. (1908). The probably error of a mean. *Biometrika*, *6*, 1–25. doi: 10.2307/2331554
- Sun, Y. Q., Hassanzadeh, P., Alexander, M. J., & Kruse, C. G. (2023). Quantifying 3D gravity wave drag in a library of tropical convection-permitting simulations for data-driven parameterizations. *J. Adv. Model. Earth. Syst.*, *15*(5), e2022MS003585. doi: <https://doi.org/10.1029/2022MS003585>
- Thiffeault, J.-L. (2012). Using multiscale norms to quantify mixing and transport. *Nonlinearity*, *84*, R1–R44. doi: 10.1088/0951-7715/25/2/R1
- Thomas, S. D. A., Jones, D. C., Faul, A., Mackie, E., & Pauthenet, E. (2021). Defining Southern Ocean fronts using unsupervised classification. *Ocean Sci.*, *17*(6), 1545–1562. doi: 10.5194/os-17-1545-2021
- Vallis, G. K. (2006). *Atmospheric and Oceanic Fluid Dynamics*. Cambridge University Press.
- Waterman, S., & Hoskins, B. J. (2013). Eddy shape, orientation, propagation, and mean flow feedback in western boundary current jets. *J. Phys. Oceanogr.*, *43*, 1666–1690. doi: 10.1175/JPO-D-12-0152.1
- Waterman, S., & Jayne, S. R. (2011). Eddy-mean flow interactions in the along-stream development of western boundary current jet: An idealized model study. *J. Phys. Oceanogr.*, *41*, 682–707. doi: 10.1175/2010JPO4477.1
- Whittle, P. (1963). Stochastic processes in several dimensions. *Bull. Int. Stat. Inst.*, *40*, 974–994.
- Young, W. R. (2012). An exact thickness-weighted average formulation of the Boussinesq equations. *J. Phys. Oceanogr.*, *42*, 692–707. doi: 10.1175/JPO-D-11-0102.1
- Yuval, J., & O’Gorman, P. A. (2020). Stable machine-learning parameterization of subgrid processes for climate modeling at a range of resolutions. *Nat. Commun.*, *11*, 3295. doi: 10.1038/s41467-020-17142-3
- Yuval, J., O’Gorman, P. A., & Hill, C. N. (2021). Use of neural networks for stable, accurate and physically consistent parameterization of subgrid atmospheric processes with good performance at reduced precision. *Geophys. Res. Lett.*, *48*, e2020GL091363. doi: 10.1029/2020GL091363
- Zanna, L., & Bolton, T. (2021). Data-driven equation discovery of ocean mesoscale closures. *Geophys. Res. Lett.*, *47*, e2020GL088376. doi: 10.1029/2020GL088376

10.1029/2020GL088376

Zhang, S., & Lin, G. (2018). Robust data-driven discovery of governing physical laws with error bars. *Proc. R. Soc. A*, *474*, 20180305. doi: 10.1098/rspa.2018.0305